

A nonlinear perspective on the
dynamics of the MJO: idealized
large-eddy simulations.

Nils P. Wedi and Piotr K. Smolarkiewicz¹

Research Department

¹National Center for Atmospheric Research, Boulder, CO80307, USA

to appear in J. Atmos. Sci.

October 2009

*This paper has not been published and should be regarded as an Internal Report from ECMWF.
Permission to quote from it should be obtained from the ECMWF.*



For additional copies please contact

The Library
ECMWF
Shinfield Park
Reading
RG2 9AX
library@ecmwf.int

Series: ECMWF Technical Memoranda

A full list of ECMWF Publications can be found on our web site under:

<http://www.ecmwf.int/publications/>

©Copyright 2009

European Centre for Medium Range Weather Forecasts
Shinfield Park, Reading, RG2 9AX, England

Literary and scientific copyrights belong to ECMWF and are reserved in all countries. This publication is not to be reprinted or translated in whole or in part without the written permission of the Director. Appropriate non-commercial use will normally be granted under the condition that reference is made to ECMWF.

The information within this publication is given in good faith and considered to be true, but ECMWF accepts no liability for error, omission and for loss or damage arising from its use.

Abstract

The 30-60 day intraseasonal atmospheric oscillation in the equatorial atmosphere, the Madden-Julian oscillation (MJO), is most visible in its signature of outgoing longwave radiation and associated convective centers. Diabatic processes related to tropical convection and two-way atmosphere-ocean interaction are hence generally believed to be crucial in explaining the origin of the MJO phenomenon. However, reliable deterministic forecasting of the MJO in global circulation models and understanding its mechanism remains unsatisfactory. Here a different approach is taken, where the hypothesis is tested that eastward propagating MJO-like structures originate fundamentally as a result of nonlinear (dry) Rossby wave dynamics. A laboratory-scale numerical model is constructed, where the generation of solitary structures is excited and maintained via zonally propagating meanders of the meridional boundaries of a zonally-periodic β -plane. The large-eddy simulations capture details of the formation of solitary structures and of their impact on the convective organization. The horizontal structure and the propagation of anomalous streamfunction patterns, a diagnostic typically used in tracing the equatorial MJO, are similar to archetype solutions of the Korteweg-deVries equation, which extends the linear shallow water theory — commonly used to explain equatorial wave motions — to a weakly nonlinear regime for small Rossby numbers. Furthermore, the characteristics of the three-dimensional laboratory-scale numerical results compare well with observed features of the equatorial MJO and thus the study provides indirect evidence of the basic principles underlying the wave-driven eastward propagation of the MJO.

1 Introduction

The Madden-Julian oscillation (MJO) ([Madden and Julian, 1971, 1972](#)) is an influential intraseasonal atmospheric fluctuation in the equatorial troposphere, resulting in slowly eastward propagating severe weather where it occurs. Therefore, the MJO is of interest to extended medium range numerical weather prediction (NWP) and climate modelling ([ECMWF, 2003](#)). It is not strictly an oscillation as its period varies and its appearance is episodic ([Hartmann and Hendon, 2007](#)). Diabatic processes associated with tropical convection and two-way atmosphere-ocean interaction are generally believed to be significant for an explanation of the MJO. Existing theories stress the importance of the feedback mechanisms between convection, large-scale dynamics and surface fluxes; see [Zhang \(2005\)](#) for a comprehensive review. However, while a synthesis of the theories and observations explains important aspects of the MJO life cycle, a unifying theory is still elusive for the basic mechanism that would also explain the ubiquitous modelling difficulties with state-of-the-art global NWP and climate models. The atmospheric processes involved appear to be of a complex, multi-scale nature ([Moncrieff, 2004](#); [Biello and Majda, 2005](#)), ranging from small-scale turbulence to convectively-driven meso-scale cloud clusters in an equatorial environment, where large-scale atmospheric waves prevail.

An intriguing aspect of modelling MJO phenomena has been reported recently by [Miura et al. \(2007\)](#) and by [Lin et al. \(2008\)](#). In the former case an MJO-like structure — albeit propagating too fast — has been simulated utilizing a “cloud-permitting” model with 7 km global grid resolution. Whereas in the latter case “no convective parametrization” global circulation model (GCM) simulations produced “one of the most realistic MJO signals in terms of variance, eastward propagation, and prominence of the spectral peak”. Because both works tend in effect to de-emphasize the role of moist convection, the present paper revisits in detail the theoretical importance of resolved nonlinear dry dynamics for MJO-like phenomena.

In particular, here the hypothesis is tested that episodic MJO-like structures propagate eastward as a result of nonlinear Rossby wave dynamics in a background flow preconditioned with lateral coupling to the extratropics. In the equatorial troposphere a correlation between eastward propagating signals and extratropical wave activity appears to be in agreement with observations and theory ([Mak, 1969](#); [Strauss and Lindzen, 2000](#); [Hoskins and Yang, 2000](#); [Straub, 2003](#)). In [Majda and Biello \(2003\)](#) a reduced set of coupled Korteweg-deVries (KDV)-like equations is derived under the assumption of weak nonlinearity. Their reduced asymptotic model

describes the fundamental (nonlinear) process of energy transfer between long-wavelength equatorially trapped baroclinic Rossby waves and barotropic Rossby waves with large meridional wavelengths in the presence of both meridional and vertical wind shear (Biello and Majda, 2004a). Importantly, solitary wave solutions are admitted by their novel equations, in which a quadratic nonlinearity $A\partial A/\partial\xi$ and a balancing dispersion term $\partial^3 A/\partial\xi^3$ of the waves' amplitude evolution (as in the classical KDV equation (8)) occur in different equations of the coupled set, resulting from the interaction of barotropic (extra-tropical) and baroclinic (equatorially trapped) wave-packets. What makes solitary wave theories with KDV-like solutions particularly attractive is that they extend the linear shallow water theory (Matsuno, 1966), commonly used to explain different modes of equatorial wave motions, to the weakly nonlinear regime. Remarkably, most or all spectral signals of satellite-observed outgoing long-wave radiation (OLR) — a proxy for cloudiness — can be explained via the linear theory of equatorially trapped waves¹, except for the dominant low-frequency spectral peak of the MJO (Wheeler and Kiladis, 1999).

There have been earlier attempts to explore the role of non-linearity for low-frequency equatorial waves (Tuyl, 1987; Zou and Cho, 2000), but their findings have been either negative or inconclusive. In an attempt to explain the anomalous eastward propagation both Tuyl (1987) and Zou and Cho (2000) tried to establish a link between a locally prescribed large-scale (internal to the tropics) diabatic heating and the dynamic evolution governed by the nonlinear shallow water equations. However, this is fundamentally different to the approach adopted in the present paper, where episodic eastward propagating solitary structures emerge as a result of the specified fluctuations of the meridional boundaries. More recently, a nonlinear view of intraseasonal oscillations in the Earth's atmosphere has been offered based on resonant triad interactions of a discrete set of planetary waves (Kartashova and L'vov, 2007). Their interpretation of intraseasonal oscillations as an intrinsic atmospheric wave phenomenon is akin to the KDV theory, as the KDV equation and triads of interacting planetary waves adopted in Kartashova and L'vov (2007) are related via the nonlinear Schrödinger equation (Boyd and Chen, 2001); the latter may be derived from quartic wave interactions (Phillips, 1981). Inasmuch as reduced models elucidate fundamental aspects of the dynamics of MJO-like phenomena, they guide the design of focused numerical experiments. Herein, numerical evidence is presented of the realizability of episodic solitary structures from nonlinear wave dynamics. As such the results substantiate the view taken in Kartashova and L'vov (2007). Moreover, the results shown offer an explanation for the ubiquitous modelling difficulties of GCMs.

The fundamental aspect of MJO dynamics isolated in this paper shows some parallelism to the investigations of Jovian vortex dynamics, and the Great Red Spot (Redekopp, 1977; Yano et al., 1997) in particular. For geophysical vortices the notion of weak non-linearity is often criticized and superseded with more general nonlinear theories of long-lived solitary vortices, namely modons (Flierl, 1987). Indeed Delaten and Yano (2009) suggest that modon theory may provide a good analog for convectively-coupled equatorial waves. Notwithstanding, Rossby solitary waves epitomize the underlying dynamical component relevant to the formation of episodic, solitary equatorial modes.

To illustrate the formation and subsequent evolution of solitary waves in a more realistic laboratory-like framework, the authors have extended their virtual laboratory for internal wave motions (Wedi and Smolarkiewicz, 2004, 2006) to the case of rotating fluids on an equatorial β -plane (Wedi and Smolarkiewicz, 2008, hereafter WS08b). In large-eddy simulations (LES) utilizing this framework, an eastward propagating large-scale Rossby solitary structure emerges after a long time compared to the time-scale of the external forcing. In the idealized setting, laterally meandering boundaries provide a translating and pulsating forcing to the equatorial flow in analogy to the lateral coupling to extratropical motions, eg. a lateral coupling to the meanderings of the subtropical jets (Charney, 1963). The forcing adopted in WS08b is similar to the one used in Malanotte-Rizzoli et al. (1988) for the study of long-lived horizontal structures observed in the vicinity of the Gulf stream meanders.

¹After Wheeler and Kiladis (1999) equatorial wave patterns in the spectral analysis of satellite-observed data records have been termed as “convectively-coupled equatorial waves”.

The organization of the paper is as follows: the next section presents the theoretical background for the MJO based on equatorial Rossby solitary waves in a horizontally inhomogeneous background flow. Section 3 describes idealized 3D β -plane simulations, shows numerical evidence of anomalous solitary structures and examines sensitivities leading to the destruction of solitary waves. Section 4 discusses the results and section 5 concludes the paper.

2 Theoretical background

In order to explain the occurrence of eastward propagating solitary horizontal structures like the MJO, we consider near-equatorial motions in a stratified fluid with long time-scales $\varepsilon_T = 1/\beta LT \ll 1$ and relatively large length-scales² $\varepsilon_L = U/\beta L^2 \ll 1$; where U, L, T denote velocity, length, and time scales respectively, and β denotes the constant latitudinal gradient of the linearized Coriolis parameter. The assumption $\varepsilon_T \ll 1$ is satisfied in the equatorial troposphere for $L \gtrsim 1000$ km and $T \gtrsim 10$ days, whereas $\varepsilon_L \ll 1$ is satisfied for $L \gtrsim 2000$ km and $U = 10$ ms⁻¹.

Before proceeding a few comments on atmospheric scales of motion in equatorial regions are in order. In [Yano and Bonazzola \(2009\)](#) the authors identify three main tropical regimes, depending on the relative importance of the Coriolis force. Because of their potential relevance to the MJO, in the following, only the first two are considered: the synoptic scale, where the Coriolis force is in balance with all other terms in the equations; and the planetary scale, where the Coriolis force is assumed to dominate over the horizontal advection. With the absence of latent heating, a vertical scale comparable to the density scale height of the atmosphere and a dominating advective time-scale $T = L/U$, synoptic-scale tropical circulations ($1000 \lesssim L \lesssim 3000$ km) are characterized by essentially barotropic, quasi-horizontal motions with small divergence of the horizontal wind ([Charney, 1963](#); [Holton, 1992](#), chap.11.2). The recent analysis of observational data ([Yano et al., 2009](#); [Yano and Bonazzola, 2009](#)) confirms and extends the relevance of this synoptic-scale regime, indicating the persistence of quasi non-divergent motions beyond the validity limits of the scale analysis. The elementary predictive tool for synoptic-scale tropical circulations, envisioned to be primarily driven by lateral coupling with extratropical and precipitating tropical motions, is the barotropic vorticity equation derived by [Charney \(1963\)](#) for Rossby numbers $Ro = U/\beta L^2 \gtrsim 1$, where U denotes a characteristic zonal velocity and L denotes a characteristic length scale.³

Planetary scales $L \gtrsim 3000$ km in the tropics are commonly viewed as dominated by linear waves — described by the linear shallow-water theory with advective terms neglected — with characteristic time scale significantly shorter than that of synoptic-scale systems ([Matsuno, 1966](#); [Gill, 1980](#); [Wheeler and Kiladis, 1999](#); [Yano and Bonazzola, 2009](#)). Consistently, a substantial part of the observed large-scale tropical variability is explained by linear equatorial wave motions. This is illustrated by the finding in [Zagar et al. \(2005\)](#) that convectively-coupled equatorial waves (cf. footnote 1) match a dominant portion of the horizontal structure of statistical deviations from a linear wave model, which is employed instead of a quasi-horizontal “balance” model⁴ for optimizing the multivariate use of observations in the ECMWF global data assimilation for NWP. However, low-frequency planetary-scale waves in the tropics, with relatively small meridional-to-zonal wavelength aspect ratio, can be described by the same barotropic vorticity equation as obtained by [Charney \(1963\)](#) for synoptic-scale motions ([Maicun, 1987b](#)).

²The geometric scales have to be sufficiently short, however, to not invalidate the β -plane assumption.

³A similar equation, for an incompressible fluid with variable depth, has been used by [Rossby \(1940\)](#) in his model of the midlatitude barotropic atmosphere ([Kuo, 1972](#)).

⁴In contrast to the geostrophic theory of midlatitudes, a balance model valid across a wide range of scales, does not exist for the tropics ([Saujani and Shepherd, 2006](#)).

The multiscale MJO model of [Biello and Majda \(2005\)](#) bridges synoptic- and planetary-scale regimes discussed above. In technical terms, the leading idea of their approach is to solve the linear equatorial planetary-scale wave equations, forced by the synoptic-scale heating fluctuations coarsened to the planetary scale. Their multiscale MJO model has successfully reproduced the vertical structure of observed MJO events. Most importantly, the analytic tractability of the underlying quasi-linear formulation makes it an attractive tool for studying selected aspects of the MJO evolution. The numerical results presented below, however, support the view taken in [Majda and Biello \(2003\)](#), [Mak \(1969\)](#) and [Charney \(1963\)](#), stressing the chronological importance of quasi-horizontal, nondivergent motions at synoptic and planetary equatorial scales, governed by the conservation of absolute vorticity. The latter view thus offers an explanation for the persistence of MJO-like structures in the absence of large heating rates — a prerequisite of the multiscale MJO model in [Biello and Majda \(2005\)](#), thought to be induced by eastward moving cloud superclusters ([Majda and Biello, 2004](#)).

The MJO possesses a characteristic length scale well above $L \sim 3000$ km ([Yano and Bonazzola, 2009](#)). Characteristic time- and length-scales of observed equatorial Rossby waves are also large with a dominant wavenumber 6 and periods of 10-15 days ([Kiladis and Wheeler, 1995](#); [Wheeler and Kiladis, 1999](#)). Motions at such large characteristic time- and length-scales thus satisfy $\varepsilon_T \ll 1$ and $\text{Ro} \equiv \varepsilon_L \ll 1$, and are governed by a barotropic potential vorticity equation, derived from an asymptotic expansion of the nonlinear shallow water equations for small Rossby number and length scales $L \sim L_R$ ([Pedlosky, 1987](#), p. 86), where $L_R = \sqrt{gH_e}/\beta L$ denotes the external Rossby deformation radius, with gravitational acceleration g and equivalent depth H_e ([Gill, 1982](#), p. 437). In contrast to the scale assumptions for linear, planetary-scale equatorial waves, the nonlinear advection terms are assumed to be of equal importance ([Pedlosky, 1987](#), p. 88) with a dominant advective time-scale L/U . In the tropics, the Rossby number of atmospheric motion is typically larger than in mid-latitudes and consequently, the nonlinear effect of advection becomes more important ([Maicun, 1987a](#)).

The quasi-geostrophic potential vorticity equation extends the shallow-water theory to a rotating, density-stratified fluid ([Pedlosky, 1987](#), ch.6.8, p.362). [Verkley \(2009\)](#) recently developed a global version of the potential vorticity equation, in which replacing the constant Coriolis parameter f_0 in the equatorial region by the variable $f = \beta y$ is justified for large-scale atmospheric flows with small horizontal divergence. Consequently, the nonlinear, quasi-horizontal evolution in a rotating, density-stratified fluid with constant Brunt-Väisällä frequency N in the equatorial β -plane is given as

$$\frac{\partial q}{\partial t} + \mathcal{J}(\psi, q + \beta y) = \eta Q, \quad (1)$$

where $\psi(x, y, z, t)$ denotes the streamfunction, and $q + \beta y$ is the potential vorticity with

$$q = \nabla^2 \psi + \sigma \mathcal{S}^{-2} \frac{\partial^2 \psi}{\partial z^2} + (\sigma - 1) \alpha \psi \quad (2)$$

as defined in [Malanotte-Rizzoli et al. \(1988\)](#). Here σ and η denote binary switches, with the values of either 1 or 0, for a stratified vs. a homogeneous shallow-water fluid and the addition of an external heating function Q ; $\mathcal{S}^2 = (L_D/L)^2$ is the squared ratio of the internal Rossby deformation radius $L_D = NH_0/\beta L$ with the characteristic horizontal length scale of the motion (H_0 is the fluid depth); $\alpha = 1/L_R^2$ is the reciprocal of the squared external Rossby deformation radius; the Jacobian operator is defined as $\mathcal{J}(a, b) = (\partial a/\partial x)(\partial b/\partial y) - (\partial a/\partial y)(\partial b/\partial x)$ and the Laplacian $\nabla^2 = \partial/\partial x^2 + \partial/\partial y^2$. Equations (1) and (2) are in nondimensional form, assuming the dimensionless variables such that

$$\begin{aligned} (x', y') &= L(x, y), z' = H_0 z, \\ t' &= (L/U)t, \psi' = UL\psi, \beta' = (U/L^2)\beta, \end{aligned} \quad (3)$$

where primes denote dimensional variables, cf. [Redekopp \(1977\)](#).

The authors in [Malanotte-Rizzoli et al. \(1988\)](#) solved equation (1) numerically, with $\sigma = \eta = 0$ and with a northern boundary forcing of the form

$$\psi(x, 1, t) = \psi_0 y_N(x, t), \quad (4)$$

using a few distinct space-and-time dependent profiles $y_N(x, t)$. In particular, a propagating and pulsating shape resulted in the emergence of self-advecting solitary structures, their “modon” regime ([Malanotte-Rizzoli et al., 1988](#)). The structures obtained in WS08b and in section 33.2, where the fully nonhydrostatic equations of motion have been employed, are consistent with the numerical solutions of (1) presented in [Malanotte-Rizzoli et al. \(1988\)](#).

Analytic solutions of the linearized form of (1) with and without topography under a specific northern boundary forcing (4) are discussed in detail in [Malanotte-Rizzoli et al. \(1987\)](#), where particular attention is given to the transition to the nonlinear regime. The full initial value problem of the nonlinear equation (1) with a northern boundary forcing is analytically intractable ([Malanotte-Rizzoli et al., 1988](#)). Notably, the linear shallow water theory of equatorially trapped waves is typically solved on the equatorial β -plane with ψ vanishing at the meridional boundaries. Equation (1) possesses linear plane-wave-form solutions for uniform zonal flow ($U = \text{const.}, V = 0$) ([Pedlosky, 1987](#), p.108) as well as periodic and solitary solutions in the asymptotic limit of weakly nonlinear dispersive waves. In the absence of a meridionally varying background flow the terms including α ensure the theoretical existence of solitary structures for the homogeneous shallow-water case ($\sigma = \eta = 0$) and for moderate Rossby radii ([Boyd, 1980](#)). The influence of a horizontally inhomogeneous background flow on the solution has been discussed in the context of midlatitude flows in [Hodyss and Nathan \(2002\)](#), where it is shown that Rossby solitary waves emerge as a result of a meridional shear of the background wind and that these waves can propagate eastward under certain conditions, thus resembling a characteristic feature of the MJO.

Given a time-independent background wind $U(x, y, z) \equiv -\partial\psi^U(x, y, z)/\partial y$ and $V(x, y, z) \equiv \partial\psi^U(x, y, z)/\partial x$; the perturbation streamfunction is

$$\Psi(x, y, z, t) = \psi(x, y, z, t) - \psi^U(x, y, z). \quad (5)$$

Considering motions with either $\alpha \ll 1$ or $\sigma \equiv 1$ and inserting (5) into (1) allows to write

$$\begin{aligned} & \left[\frac{\partial}{\partial t} + U \frac{\partial}{\partial x} + V \frac{\partial}{\partial y} \right] (\nabla^2 \Psi + \sigma \mathcal{L}^{-2} \frac{\partial^2 \Psi}{\partial z^2}) \\ & + \mathcal{J}(\Psi, \nabla^2 \Psi + \sigma \mathcal{L}^{-2} \frac{\partial^2 \Psi}{\partial z^2}) \\ & + \mathcal{J} \left(\Psi, \frac{\partial V}{\partial x} - \frac{\partial U}{\partial y} + \beta y + \sigma \mathcal{L}^{-2} \frac{\partial^2 \Psi^U}{\partial z^2} \right) = \eta \mathcal{Q}', \end{aligned} \quad (6)$$

where the background streamfunction is required to satisfy

$$\mathcal{J} \left(\Psi^U, \frac{\partial V}{\partial x} - \frac{\partial U}{\partial y} + \beta y + \sigma \mathcal{L}^{-2} \frac{\partial^2 \Psi^U}{\partial z^2} \right) = \eta \bar{Q}, \quad (7)$$

and $\mathcal{Q}' = \mathcal{Q} - \bar{Q}$ denotes a perturbation of the external heating with respect to the background state $\bar{Q}(x, y, z)$. Considering relation (5), the streamfunction solution of (6) may be interpreted as the evolution of a time-mean anomaly, that is, the spatio-temporal deviation from the time-averaged streamfunction, if (i) the time-mean field satisfies (7); and (ii) the time-mean of the self-interaction term $\mathcal{J}(\Psi, \nabla^2 \Psi + \sigma \mathcal{L}^{-2} \partial^2 \Psi / \partial z^2)$ is small. Notably, it is this self-interaction term that provides the essential nonlinearity, necessary to obtain solitary wave solutions. An evolution equation for the amplitude of solitary waves (i.e. a KDV equation) can be derived from equation (6) for weakly nonlinear dispersive waves ([Hodyss and Nathan, 2002](#); [Dodd et al., 1982](#), chap. 2 and references therein). Although the derivation of the potential vorticity equation (1) is based on an asymptotic

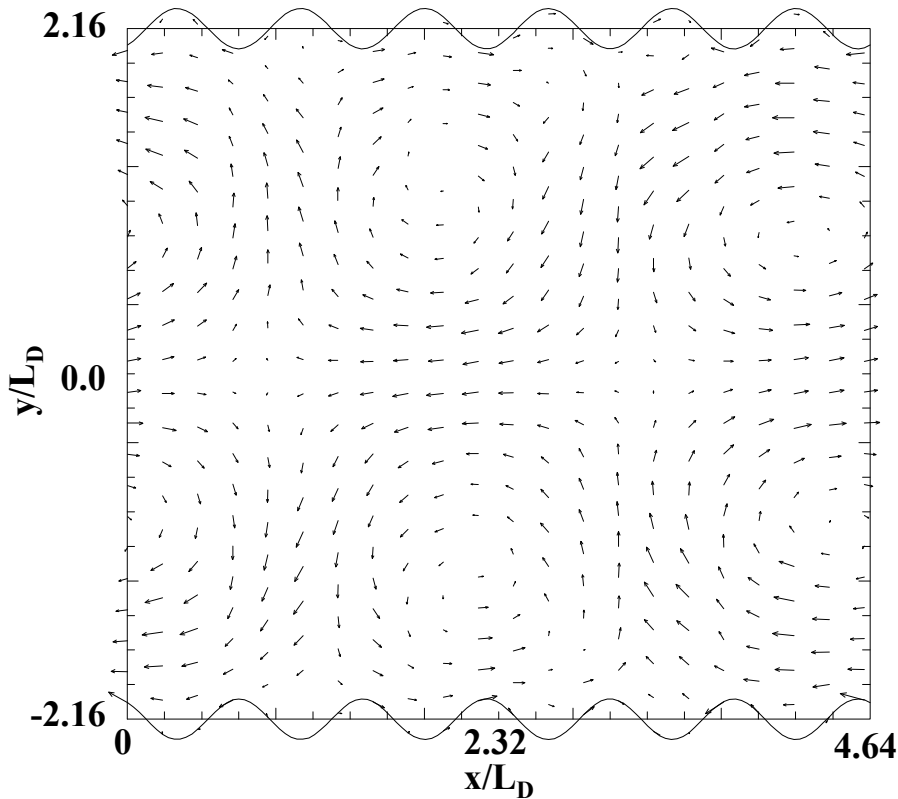


Figure 1: Instantaneous temporal anomaly of wind (vectors) in the nonlinear 2D simulation with a propagating and meridionally pulsating lateral forcing as described by eq. (11).

expansion for small Rossby number, it has been shown in [Malanotte-Rizzoli \(1980\)](#) that the permanence of solitary structures persists beyond the validity of the analytic theory upto $Ro \rightarrow 1$, after which a transition from wave-like to turbulent behavior ensues.

In WS08b the multi-scale anelastic research code EULAG ([Prusa et al., 2008](#)) was introduced with a pulsating and zonally propagating meridional boundary meander. Suitably modified — by assuming an incompressible fluid confined between free-slip rigid-lid boundaries and no variability in the vertical — it has been employed to mimic the nonlinear barotropic shallow water equations on a zonally-periodic β -plane. Using this 2D model the authors reported a robust low-wavenumber and low-frequency anomalous signature in the results, thought to be induced by the boundary meander. Figure 1 shows a snapshot of the instantaneous anomalous flow field in the 2D simulation with the meridional boundary meander, specified later in eq. (11). The anomaly has been calculated with respect to the time-mean field. The anomalous counter-rotating vortices are pulsating and progressing eastward. In the 2D simulation, a quadrupole structure forms first and persists for some time, to later change into a single pair of anomalous counter-rotating vortices. With a single-sided forcing smaller anomalous vortices can be seen to merge into a single, larger anomalous flow vortex that is maintained throughout the simulation unless the lateral forcing is stopped. In the latter case we find that the vortex propagates for a while and then dissipates. This is in agreement with the results found in [Malanotte-Rizzoli et al. \(1988\)](#), where such a vortex depending on the nonlinearity of the forcing can persist for a long time against the effects of dispersion (numerical or physical).

The horizontal structure found in the 2D simulation corresponds to the prototype Rossby soliton (cf. Fig. 2 of

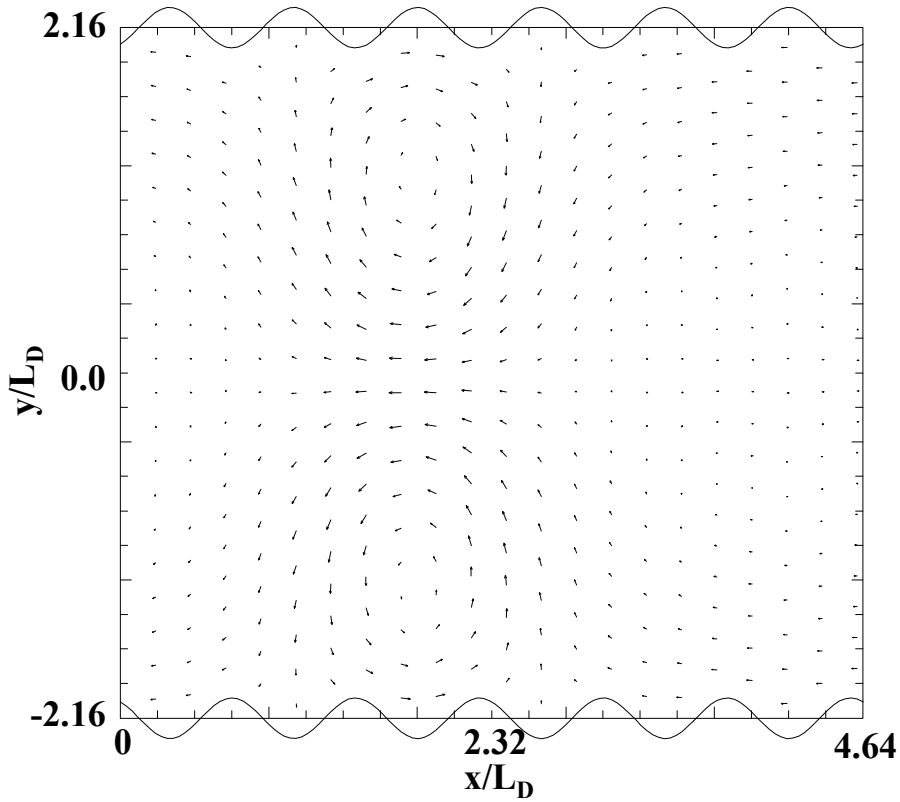


Figure 2: Instantaneous temporal anomaly of wind (vectors) obtained from a weakly-nonlinear analytic streamfunction solution of the KDV equation (8) with time mean coefficients $\mu = -1.51$, $\gamma = -0.043$, and $\delta = +0.05$. The solution utilized the time-mean zonally-averaged background wind $U^{(0)}$ from the 2D numerical simulation.

Boyd (1980)) — a solution of the KDV equation

$$\frac{\partial A}{\partial \tau} + \delta \frac{\partial A}{\partial \xi} + \mu A \frac{\partial A}{\partial \xi} + \gamma \frac{\partial^3 A}{\partial \xi^3} = 0, \quad (8)$$

where A describes the amplitude evolution, in zonal direction ξ and in time τ , of the streamfunction anomaly $\Psi^{(1)} = A(\xi, \tau)Y^{(1)}(y)$, where $Y^{(1)}$ is a meridional structure function found by solving $Y_{yy}^{(1)} + [(\beta - U_{yy}^{(0)})/(U^{(0)} - c_0)]Y^{(1)} = 0$ and δ, μ, γ are non-dimensional coefficients (cf. Fu et al. (2005)); $U^{(0)}$ denotes the time-mean zonally-averaged background wind and $c_0 = -\beta/(k^2 + l^2)$ is the linear Rossby wave's propagation speed, and k, l denote zonal and meridional wavenumbers, respectively. The horizontal structure of solitary Rossby waves is anisotropic with meridional winds weaker in comparison to the zonal winds near the equator. An analytic solution of the KDV equation (8) is obtained with the time mean coefficients $\mu = -1.51(0.02)$, $\gamma = -0.043(0.0001)$, and $\delta = +0.05(0.082)$, where the values in parentheses indicate the standard deviations. The computation of the coefficients and of the meridional structure function utilized the time-mean zonally-averaged background wind $U^{(0)}$ from the 2D numerical simulation; $Y^{(1)}$ is found $\propto H_n(y)e^{-y^2}$ with $H_n(y)$ denoting the n th Hermite polynomial, characteristic of equatorially trapped waves (Matsuno, 1966; Boyd, 1980). The analytic solution using the time mean coefficients (Fig. 2) reproduces a pair of eastward propagating anomalous counter-rotating vortices. While the structure of the anomaly is comparable to those in the 2D numerical results, the amplitude of the zonal velocities and the propagation speed is much larger in the analytic solution. Furthermore, the anomalous time-variation of the coefficient δ

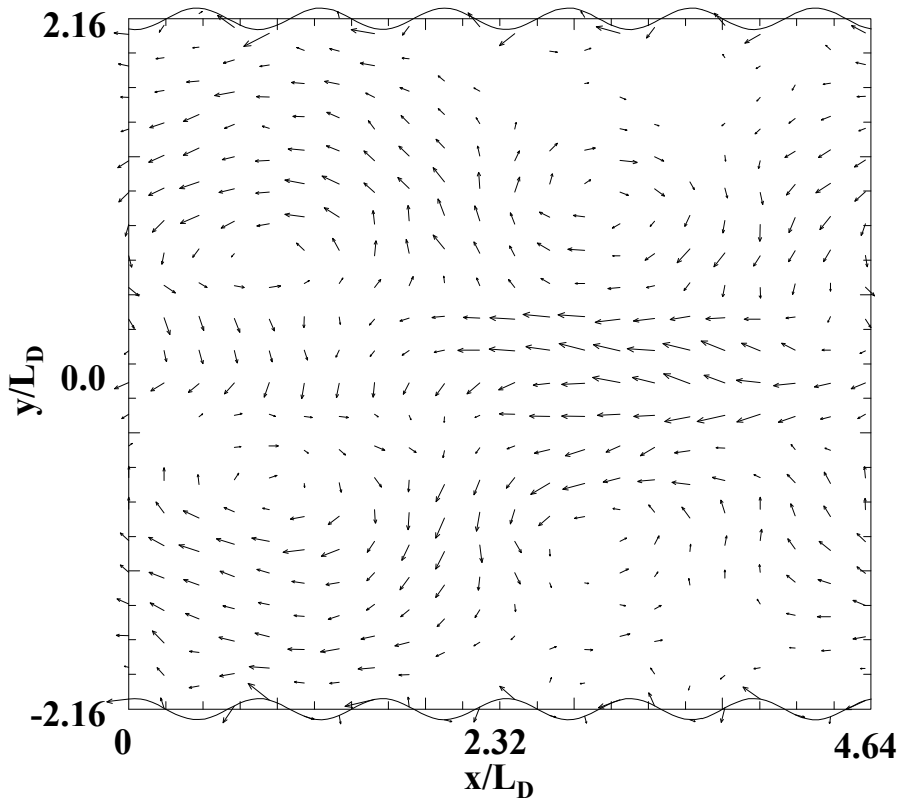


Figure 3: Temporal anomaly of wind (vectors) after $t^* \equiv U/L_D t = 797$ in the 3D simulation at 0.04 m height (approx. $0.4H_0$) with a propagating and meridionally pulsating lateral forcing as described by eq. (11).

is inconsistent with the slow time-scale assumed for the KDV theory. In conclusion, although a simple KDV model illustrates some aspects of solitary equatorial dynamics, the discrepancies between the analytic and the fully nonlinear numerical results are significant. Nevertheless, Rossby solitary structures are a distinct feature of the large-eddy simulations presented in the next section.

3 Large-eddy simulations on the equatorial β -plane

The laboratory experiment of [Plumb and McEwan \(1978\)](#) and their numerical equivalents ([Plumb and Bell, 1982](#); [Wedi and Smolarkiewicz, 2005, 2006](#)) were shown to be useful tools for understanding geophysical phenomena in a controlled environment. Hence the realizability of episodic solitary structures in a fully nonlinear three-dimensional flow is first established in such an idealized framework before attempting to explain their occurrences in nature, and before attempting to comment on the difficulty of their simulation in GCMs. The β -plane model introduced in WS08b serves here as an analogous tool. Despite its simplification with respect to natural atmospheric processes the model incorporates convective motions, externally driven large-scale dynamics and surface boundary layer fluxes due to imposed heating and friction. It thus implements and sufficiently enriches the reduced MJO models of the previous section, to substantiate the hypothesis that, under certain conditions, eastward propagating solitary structures emerge and match the characteristic dynamics of the equatorial MJO.

3.1 Numerical model

The Boussinesq equations of motion for a rotating, density-stratified fluid shown in WS08b are cast here in a time-dependent curvilinear framework (Prusa and Smolarkiewicz, 2003; Smolarkiewicz and Prusa, 2005; Wedi and Smolarkiewicz, 2004):

$$\begin{aligned} \frac{\partial(\rho^* \bar{v}^{s^k})}{\partial \bar{x}^k} &= 0, \\ \frac{dv^j}{d\bar{t}} &= -\tilde{G}_j^k \frac{\partial \pi'}{\partial \bar{x}^k} - g \frac{\rho'}{\rho_0} \delta_3^j + \mathcal{C}^j + \mathcal{F}^j, \\ \frac{d\rho'}{d\bar{t}} &= -\bar{v}^{s^k} \frac{\partial \rho_e}{\partial \bar{x}^k} + \mathcal{F}_\rho. \end{aligned} \quad (9)$$

Here, $\rho^* := \rho_0 \bar{G}$, with \bar{G} denoting the Jacobian of the transformation between physical (t, x, y, z) and computational $(\bar{t}, \bar{x}, \bar{y}, \bar{z})$ space. Indices $j, k = 1, 2, 3$ correspond to the $\bar{x}, \bar{y}, \bar{z}$ components, respectively; summation is implied by repeated indices, unless stated otherwise. The total derivative is $d/d\bar{t} = \partial/\partial \bar{t} + \bar{v}^{s^j} (\partial/\partial \bar{x}^j)$, where $\bar{v}^{s^j} := \bar{x}^j$ denotes the contravariant velocity in the transformed framework. The solenoidal velocity, satisfying the mass continuity equation in (9), is $\bar{v}^{s^j} := \bar{v}^{s^j} - \partial \bar{x}^j / \partial t$. The components of physical velocity v^j are related via $\bar{v}^{s^k} = \tilde{G}_j^k v^j$, where $\tilde{G}_j^k = (\partial \bar{x}^k / \partial x^j)$ are the transformation coefficients in the computational space. The particular mapping employed assumes identity transformations $\bar{t} = t$, $\bar{x} = x$ and $\bar{z} = z$, but

$$\bar{y} = y_0 \frac{y - y_S(x, y, t)}{y_N(x, y, t) - y_S(x, y, t)}, \quad (10)$$

where y_S and y_N are the southern and northern domain boundaries, respectively; and y_0 denotes the domain size in meridional direction. Numerically, the elements of the Jacobi matrix are evaluated in (\bar{t}, \bar{x}) leading to the required subset of (non-trivial) coefficients $\tilde{G}_1^1 = \mathcal{G}^{-1} \partial y / \partial \bar{y}$, $\tilde{G}_1^2 = \mathcal{G}^{-1} \partial y / \partial \bar{x}$, $\tilde{G}_2^1 = \mathcal{G}^{-1} \partial x / \partial \bar{y}$, and $\tilde{G}_2^2 = \mathcal{G}^{-1} \partial x / \partial \bar{x}$ with $\mathcal{G}^{-1} = (\partial y / \partial \bar{y} \partial x / \partial \bar{x} - \partial y / \partial \bar{x} \partial x / \partial \bar{y})^{-1}$; cf. Wedi and Smolarkiewicz (2004) for details. The ρ' and π' denote, respectively, density and normalized-pressure perturbations with respect to the ambient state characterized by the geostrophic wind components v_e^j and the linearly stratified profile $\rho_e = \rho_0(1 - (N^2/g)z)$; g symbolizes the gravitational acceleration, ρ_0 is a constant reference density, and N denotes the Brunt-Väisälä frequency; δ_3^j is the Kronecker delta. Note that the ambient zonal flow u_e (cf. table 1) is used together with the boundary meander to mimic an extra-tropical anomalous flow between 600hPa-200hPa. The Coriolis-force terms on the equatorial β -plane⁵ are given as $\mathcal{C}^1 = +\beta y(v^2 - v_e^2)$, $\mathcal{C}^2 = -\beta y(v^1 - v_e^1)$, and $\mathcal{C}^3 = 0$. Diabatic and frictional terms emulating boundary layers adjacent to $r = y, z$ boundaries are of the form $\mathcal{F}_\rho(r) := \tau_\rho^{-1} e^{-r/h} (\rho - \rho_b)$ and $\mathcal{F}^j(r) := \tau_{v^j}^{-1} e^{-r/h} (v^j - v_b^j)$, with subscript b denoting a prescribed boundary value; the attenuation time scales are $\tau_\rho = \Delta z^2 / \kappa$ and $\tau_{v^j} = 0.125 \tau_\rho$ (assuming diffusivity of heat in water, $\kappa = 1.39 \times 10^{-7} \text{ m}^2 \text{ s}^{-1}$) and height scale $h = 2\Delta z$, where Δz is the vertical gridsize. Given the model's formulation in density, heating is included indirectly via the gradient of density at the lower boundary, which induces convective vertical motions. Weak, moderate and strong heating is defined by the boundary value of the density ratio $(\rho_0 - \rho_b) / \rho_b = 0.0016, 0.0048$ and 0.0096 , respectively. The velocity values at the lower and lateral boundaries are set to zero ($v_b^j = 0$) unless specified otherwise. The upper boundary is freeslip, with $\mathcal{F}^j(z = H_0) = 0$ and $\mathcal{F}_\rho(z = H_0) = 0$.

The governing equations (9) are discretized in the transformed space using a second-order-accurate, flux-form Eulerian, nonoscillatory forward-in-time approach, see Smolarkiewicz and Szmelter (2009) for a recent discussion. All prognostic equations in (9) are integrated consistent with the trapezoidal rule, treating the inviscid adiabatic dynamics on the rhs implicitly. Frictional and heating terms are computed explicitly, to the

⁵The shallow atmosphere (or ‘‘traditional’’ approximation) has been applied here for consistency with simulations using the Integrated Forecasting System (IFS), the operational global forecast model at ECMWF; see also Wedi and Smolarkiewicz (2009).

first order. Together with the curvilinearity of the coordinates, (9) leads to a complicated elliptic problem for pressure (see Appendix A in Prusa and Smolarkiewicz, 2003, for the complete description) solved iteratively using the preconditioned generalized conjugate-residual approach — a nonsymmetric Krylov-subspace solver (Smolarkiewicz et al., 2004).

The simulations described here broadly fit into the class of implicit large-eddy simulations (ILES). ILES dispenses with explicit subgrid-scale models and exploits truncation properties of high resolution (non-oscillatory) finite-volume methods to mimic the spectral viscosity of standard LES (Domaradzki et al., 2003; Margolin et al., 2006; Piotrowski et al., 2009).

The experiment is set in a zonally-periodic, equatorial β -plane. The simulations are represented by $128 \times 128 \times 64$ gridpoints and the experimental parameters and their corresponding atmospheric values (discussed in the text) are summarized in table 1. The characteristic scales L, U, β', H_0 are used in the non-dimensionalization (3) to equivalence laboratory-scale and atmospheric-scale motions in terms of the Rossby (Ro) and Richardson (Ri = $N^2 H_0^2 / U^2 = \mathcal{O}(10)$) numbers and flow Froude number ($\text{Fr}^2 = U^2 / g H_0 \ll 1$). All times, as well as zonal and meridional lengths are normalized in the following by T_D and L_D , respectively.

Table 1: Experimental parameters.

Symbol	Laboratory Scale	Atmospheric Scale	Description
L	2 m	4000 km	length-scale
U	0.05 ms^{-1}	50.0 ms^{-1}	velocity-scale
β'	$0.093 \text{ m}^{-1} \text{ s}^{-1}$	$2.3 \times 10^{-11} \text{ m}^{-1} \text{ s}^{-1}$	Coriolis β
N	1.566 s^{-1}	0.01 s^{-1}	Brunt-Väisällä frequency
$u_e, (v_e = 0, w_e = 0)$	0.05 ms^{-1}	50.0 ms^{-1}	ambient flow
x_0	4.3 m	8600 km	zonal domain length
y_0	4.0 m	8000 km	meridional domain width
H_0	0.11 m	17000 m	vertical domain height
T_1, T_2	120 s, 100 s	2.7 days, 2.3 days	forcing periods
a	0.2 m	400 km	forcing amplitude
$\lambda = x_0 / s (s = 6)$	0.717 m	1430 km	forcing wavelength
$L_D = N H_0 / \beta L$	0.926 m	1850 km	equatorial deformation radius
$T_D = L_D / U$	18.5 s	10 hours	equatorial deformation time

The model uses a timestep $\Delta t = 0.1 \text{ s}$ and is run for up to eight hours or $t^* = t / T_D \approx 1555$. Given an equatorial deformation time $T_D \approx 10$ hours in the Earth tropics, the simulations represent a laboratory-scale ‘climate’ realization.

The meridional boundaries are specified by the superposition of two waves with frequencies $\omega_1 = 2\pi / T_1$ and $\omega_2 = 2\pi / T_2$,

$$y_S(x, y, t) = -\frac{y_0}{2} + a \cos\left(\frac{\omega_2 - \omega_1}{2} t\right) \sin\left(k_x x - \frac{\omega_1 + \omega_2}{2} t\right), \quad (11)$$

and $y_N(x, y, t) = -y_S(x, y, t)$, where y_0 denotes the domain size in meridional direction (and analogously x_0 specifies the domain size in zonal direction) and $k_x = 2\pi / \lambda$ with zonal wavelength λ . Such a forcing prescribes a

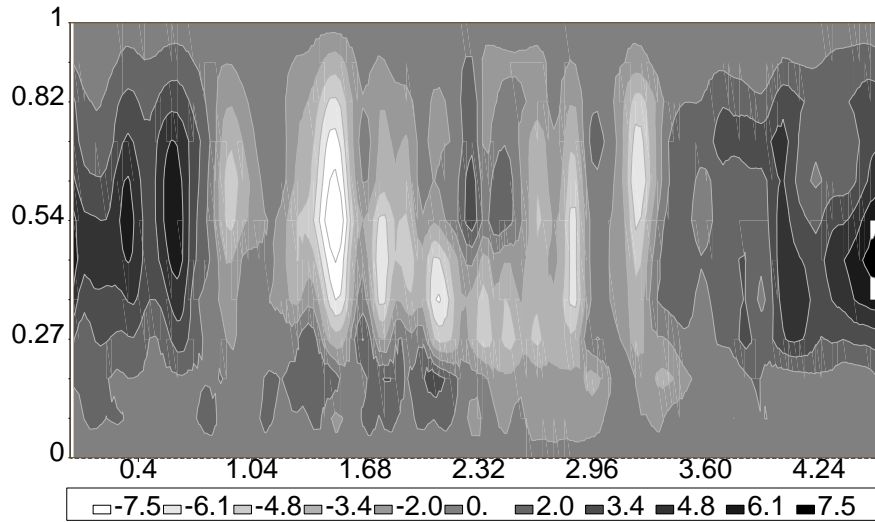


Figure 4: Vertical cross section of vertical velocity (meridionally averaged over the near equatorial region $\pm 0.844L_D$ from the mid-channel ($y = 0$)) at $t^* = 797$ for the simulation of a stably stratified flow with uniform bottom heating ($\mathcal{F}_\rho \neq 0$) and boundary layer friction ($\mathcal{F}^j \neq 0$) included. Contours are ($\times 10^{-5} \text{ m s}^{-1}$).

boundary meander (a similar forcing is provided in case d of table 1 in [Malanotte-Rizzoli et al., 1988](#)) propagating eastward with the mean phase velocity $(\omega_1 + \omega_2)/2k_x$ and pulsating with the frequency $(\omega_2 - \omega_1)/2$. Unless specified otherwise the boundary forcing is active in the period $108 < t^* < 1555$ and the forcing amplitude a is one tenth of the meridional extent of the domain. Equations (11) together with (9) allow for a time-dependent meridional boundary forcing free of small-amplitude approximations.

3.2 Results

The principal result is that the meridional undulations (11) generate a long-lived, anomalous structure that corresponds to a robust low-wavenumber and low-frequency signature in the wave-spectra obtained.

In the 3D simulations that include stratification and thermal forcing, the flow field is more complex than in the 2D results alluded to earlier. Figure 3 shows the instantaneous eastward propagating anomalous wind (vectors) at $\approx 0.4H_o$ (0.04 m height) after $t^* = 797$. The velocity vectors are $\mathcal{O}(u_e)$ as in the 2D numerical results in Fig. 1. Similar to the 2D simulations both a single pair of vortices as well as a quadrupole structure persists at different times. The near-equatorial easterly anomaly seen in Fig. 3 prevails upto $\approx 0.6H_o$. At levels below, the equatorial wind is flanked by two counter-rotating vortices located nearer to the equator. Higher up a broader quadrupole structure spanning the whole meridional extent of the domain is more evident (not shown). Overall the 3D organization is reminiscent of Fig. 6a in [Moncrieff \(2004\)](#). The corresponding anomalous vertical structure is displayed in Fig.4. Broad areas of dark and light shading denote upward and downward vertical motions, respectively. The upper panel in Fig. 5 shows the corresponding Hovmöller diagram of the eastward moving temporal anomaly of velocity potential⁶ at $0.4H_o$ height. The dark contours indicate negative velocity potential and light contours denote positive velocity potential. The latter corresponds to the center-left of the Rossby solitary wave structure, Fig. 3, and is associated with upward vertical motions, Fig.4.

Deep convection — here defined as the dry, buoyancy-driven vertical motions resulting from the prescribed near-surface density gradient — develops randomly until $t^* = 108$ in the simulation, before starting the oscillation.

⁶Velocity potential anomalies are a common tracer of the MJO. However, it has been shown in [Chen and Chen \(1997\)](#) that velocity potential and streamfunction may be used equivalently, as both propagate eastward coherently for the equatorial MJO.

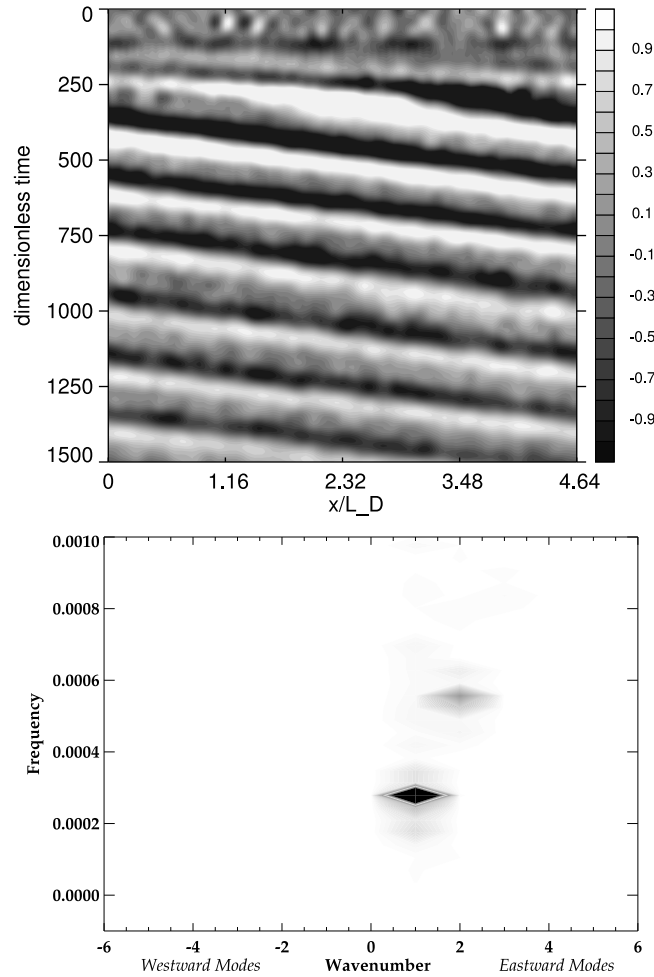


Figure 5: Hovmöller diagrams of the temporal anomaly of velocity potential ($\times 10^{-5} \text{ m}^2 \text{ s}^{-1}$) at $0.4H_o$ for the simulation of a stably stratified flow with uniform bottom heating ($\mathcal{F}_p \neq 0$) and boundary layer friction ($\mathcal{F}^j \neq 0$) at the bottom and the lateral walls included. The upper panel shows the simulation with a continuous lateral boundary oscillation (after $t^* = 108$). The Hovmöller data has been averaged over the near equatorial region $\pm 0.844L_D$ from the mid-channel ($y = 0$) and lowpass filtered, to attenuate all frequencies larger and equal to the beat frequency of the boundary oscillation $(\omega_2 - \omega_1)/2$. The lower panel shows the wavenumber-frequency analysis. The frequency displayed is the inverse period $\omega/2\pi$. The spectral analysis as well as the computation of the temporal mean involved the full simulation period $0 < t^* < 1555$. Both time and the zonal length are nondimensionalized using the internal Rossby radius of deformation L_D .

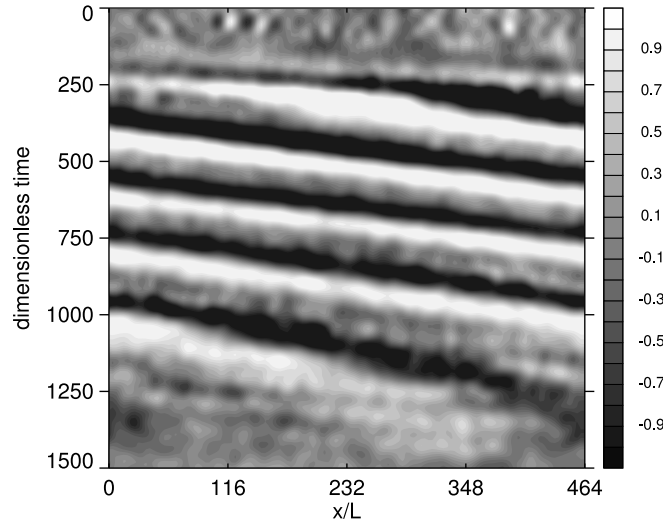


Figure 6: Hovmöller diagram of the temporal anomaly of velocity potential ($\times 10^{-5} \text{ m}^2 \text{ s}^{-1}$) at $0.4H_0$ same as in Fig. 5 but for the simulation where the lateral boundary oscillation is stopped at $t^* = 762$.

tion of the lateral boundaries. This initial stage can be clearly distinguished by the regime change in Fig. 5 with the onset of zero or negative velocity potential. Judging from Fig. 5 it takes approximately 140 dimensionless time units after the start of the boundary oscillations, before the first solitary structure emerges. Initially higher wavenumber modes are present. The wavenumber-frequency diagram of velocity potential in the lower panel of Fig. 5 confirms a dominant eastward propagating wavenumber one mode in the 3D simulation with periods⁷ of approximately $T^* = 194$. This period is significantly longer than the periods associated with the beat frequency and the individual forcing frequencies of the boundary, and longer than the period obtained from the linear dispersion relationship for a wavenumber one Rossby wave. After the solitary wave has fully developed in the 3D simulation the eastward propagating Rossby solitary structure persists until $t^* = 1555$ dimensionless time units, at which the simulation was stopped (Fig. 5). When the meridional boundary meander was stopped at $t^* = 762$, the solitary wave equally continued to propagate eastward until approximately $t^* = 1300$, showing an extraordinary persistence (Fig. 6).

A series of simulations — summarized in table 2 — has been run to explore parametric sensitivities. Both the specified boundary forcing and the meridional variation of the Coriolis force are found to be necessary for attaining long-lived, large-scale solitary structures. There are, however, other sensitivities that prevent the development of an anomalous solitary structure despite otherwise favorable conditions. First, if the fluid is neutrally stratified no dominant low-frequency eastward or westward propagation (Fig. 7) is observed. Instead a broad range of frequencies is found, unless the meridional extent of the domain is decreased to $y_0 \approx 1.6L_D$ or below, in which case the boundary forcing frequency⁸ becomes dominant.

In simulations with stable stratification but in the absence of all frictional and heating terms ($\mathcal{F}^j \equiv \mathcal{F}_\rho \equiv 0$) a propagating wavenumber one signal is not observed. While heating or friction imposed at the lateral boundaries has little effect on the formation of solitary structures, further experiments show that the occurrence of solitary wave solutions is quite sensitive to imposed variations in the boundary conditions at $z = 0, H_0$. For example, noslip upper boundary conditions weaken the eastward propagating signal. More importantly, if either $\mathcal{F}^j \neq 0$ or $\mathcal{F}_\rho \neq 0$ or both are different from zero at the lower boundary, eastward propagating solitary waves are ob-

⁷Given the periodicity of the domain, period refers to the time required for an anomalous solitary structure to propagate eastward and return to the same longitudinal position.

⁸The spectral signal of the boundary forcing (with periods 100, and 120 seconds) cannot be seen in the figures even if the data is unfiltered, since the postprocessing interval for the 3D data — underlying the spectral analysis — is 60 s.

Table 2: Summary of parametric sensitivity studies discussed in the text; the symbols and their units are defined in table 1 and section 33.1.

Sensitivity	N^2/g	$(\rho_0 - \rho_b)/\rho_b$	\mathcal{F}^J	a	λ	ω_1, ω_2	β	Figure
Control	0.25	0.0016	$\neq 0$	0.2	0.717	100, 120	0.093	3, 4, 5, 6, 11
No Coriolis	0.25	0.0016	$\neq 0$	0.2	0.717	100, 120	0	—
No stratification	0	0.0016	$\neq 0$	0.2	0.717	100, 120	0.093	7, 11
No stratification	0	0	0	0.2	0.717	100, 120	0.093	—
Stratification	$1. \times 10^{-4}$	0	0	0.2	0.717	100, 120	0.093	—
Stratification	$1. \times 10^{-2}$	0	0	0.2	0.717	100, 120	0.093	—
No bottom friction	0.25	0	0	0.2	0.717	100, 120	0.093	11
No bottom friction	0.25	0.0016	0	0.2	0.717	100, 120	0.093	—
No bottom friction	0.25	0.0048	0	0.2	0.717	100, 120	0.093	8, 9, 11
No bottom heating	0.25	0	$\neq 0$	0.2	0.717	100, 120	0.093	10a, 10b
Bottom heating	0.25	0.0048	$\neq 0$	0.2	0.717	100, 120	0.093	10c, 10d
Bottom heating	0.25	0.0096	$\neq 0$	0.2	0.717	100, 120	0.093	10e, 10f, 11
Forcing amplitude	0.25	0.0016	$\neq 0$	0	0.717	100, 120	0.093	—
Forcing amplitude	0.25	0.0016	$\neq 0$	0.4	0.717	100, 120	0.093	—
Forcing amplitude	0.25	0.0016	$\neq 0$	0.05	0.717	100, 120	0.093	—
Forcing amplitude	0.25	0.0016	$\neq 0$	0.005	0.717	100, 120	0.093	—
Forcing wavelength	0.25	0.0016	$\neq 0$	0.2	0.926	100, 120	0.093	—
Forcing wavelength	0.25	0.0016	$\neq 0$	0.2	0.0926	100, 120	0.093	—
Forcing frequency	0.25	0.0016	$\neq 0$	0.2	0.717	100, —	0.093	—
Forcing frequency	0.25	0.0016	$\neq 0$	0.2	0.717	random	0.093	—
Forcing frequency	0.25	0.0016	$\neq 0$	0.2	0.717	$y_S \neq -y_N$	0.093	—

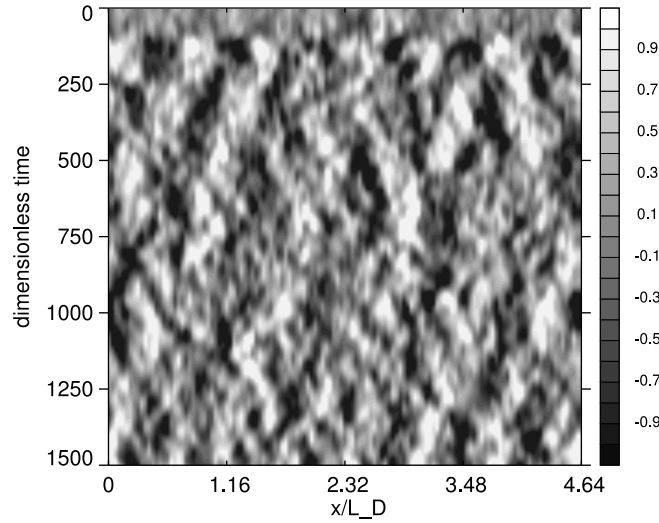


Figure 7: Hovmöller diagram of the temporal anomaly of velocity potential ($\times 10^{-4} \text{ m}^2 \text{ s}^{-1}$) at $0.4H_o$ as in Fig. 5 but for the neutrally stratified case. Velocity potential is rescaled $\times 10$ for plotting.

served in the 3D simulations, cf. Figs. 8 and 10 a-b. If the reference simulation (cf. Figs. 4 and 5) is simplified by eliminating just the frictional bottom boundary layer, the simulation still develops a dominant eastward wavenumber one mode (Fig. 8). Notably, if the oscillating boundary meander is stopped after $t^* = 762$ in this simulation, the solitary structure continues to persist until $t^* = 1555$ (not shown), when the simulation was stopped. Figure 9 shows a typical cross section of vertical velocity at $t^* = 849$, averaged between $\pm 0.844L_D$. One can identify deep upward and downward vertical motions within the eastward propagating envelope between $0.4 - 1.68L_D$, but suppressed otherwise. This particular region is characterized by an anomalous positive velocity potential that is part of a solitary wave structure similar to the one depicted in Fig. 3.

In the absence of bottom heating (Fig. 10 a-b) the eastward propagation speed of the flow anomaly is the same compared to the simulation with bottom heating depicted in Fig. 5, but the amplitude is weaker. In Fig. 10, panels c-f the same friction $\mathcal{F}^j \neq 0$ as in the simulation of Fig. 5 is applied. With moderate bottom heating the solitary structure is retained (Fig. 10 panels c-d) but it propagates faster. When the magnitude of the imposed bottom boundary layer heating is increased further, the signature of the anomalous flow pattern weakens (Fig. 10, panels e-f) and becomes more episodic, while convective vertical motions and higher horizontal wavenumbers dominate. With strong heating the corresponding vertical mixing is enhanced leading to zero static stability, as in the neutrally stratified case, and the disappearance of the dominant propagating low-frequency signal.

Figure 11 illustrates the zonal mean zonal wind shear in meridional (upper panel) and in vertical (lower panel) direction for selected simulations. Both the strongly stratified simulation with no bottom friction or heating ($\mathcal{F}^j \equiv \mathcal{F}_\rho \equiv 0$) and the neutrally stratified simulation are characterized by the absence of a vertical shear of the zonal mean wind and do not show a significant wavenumber one signal. In addition, there is no significant meridional shear of the zonal mean wind in the neutrally stratified case but there is a meridional shear in the case with no bottom friction or heating. The simulation with strong bottom heating has a vertical as well as a meridional shear of zonal mean zonal wind but no significant wavenumber one signal (cf. Fig. 10 f). Further, the simulation with bottom heating ($\mathcal{F}_\rho \neq 0$) but no frictional bottom boundary layer imposed ($\mathcal{F}^j = 0$) does not show a significant vertical shear, yet develops a strong wavenumber one signal. In summary, neither a meridional nor a vertical shear of the zonal mean wind are sufficient for the occurrence of a low-frequency wavenumber one signal. However, a meridional shear of the zonal mean zonal wind appears to be a necessary condition for the occurrence of a low frequency signal in our simulations.

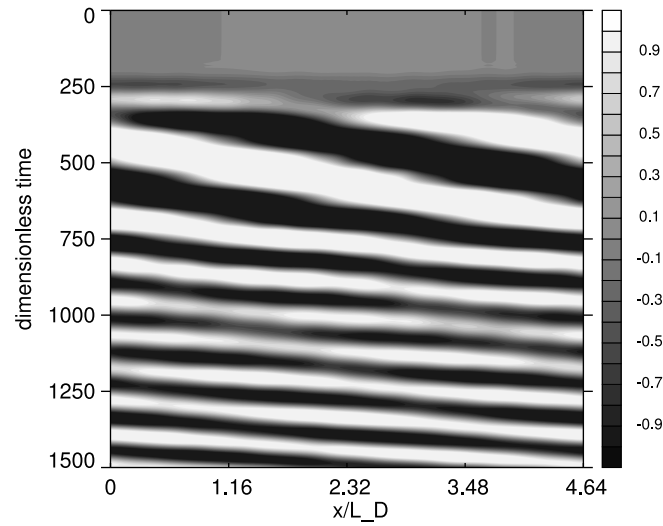


Figure 8: Hovmöller diagram of the temporal anomaly of velocity potential ($\times 10^{-5} \text{ m}^2 \text{ s}^{-1}$) at $0.4H_o$ as in Fig. 5 but for the simulation of a stably stratified flow with bottom heating ($\mathcal{F}_p \neq 0$) and no frictional bottom boundary layer imposed ($\mathcal{F}^j = 0$)

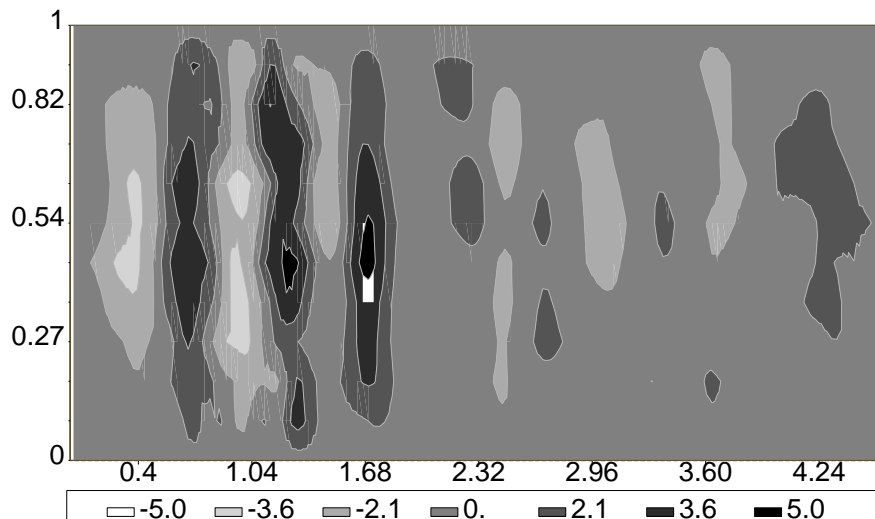


Figure 9: Vertical cross section of vertical velocity (meridionally averaged as in Fig. 4) at $t^* = 849$ for the simulation of a stably stratified flow with bottom heating ($\mathcal{F}_p \neq 0$) and no frictional bottom boundary layer imposed ($\mathcal{F}^j = 0$). Contours shown are ($\times 10^{-4} \text{ ms}^{-1}$).

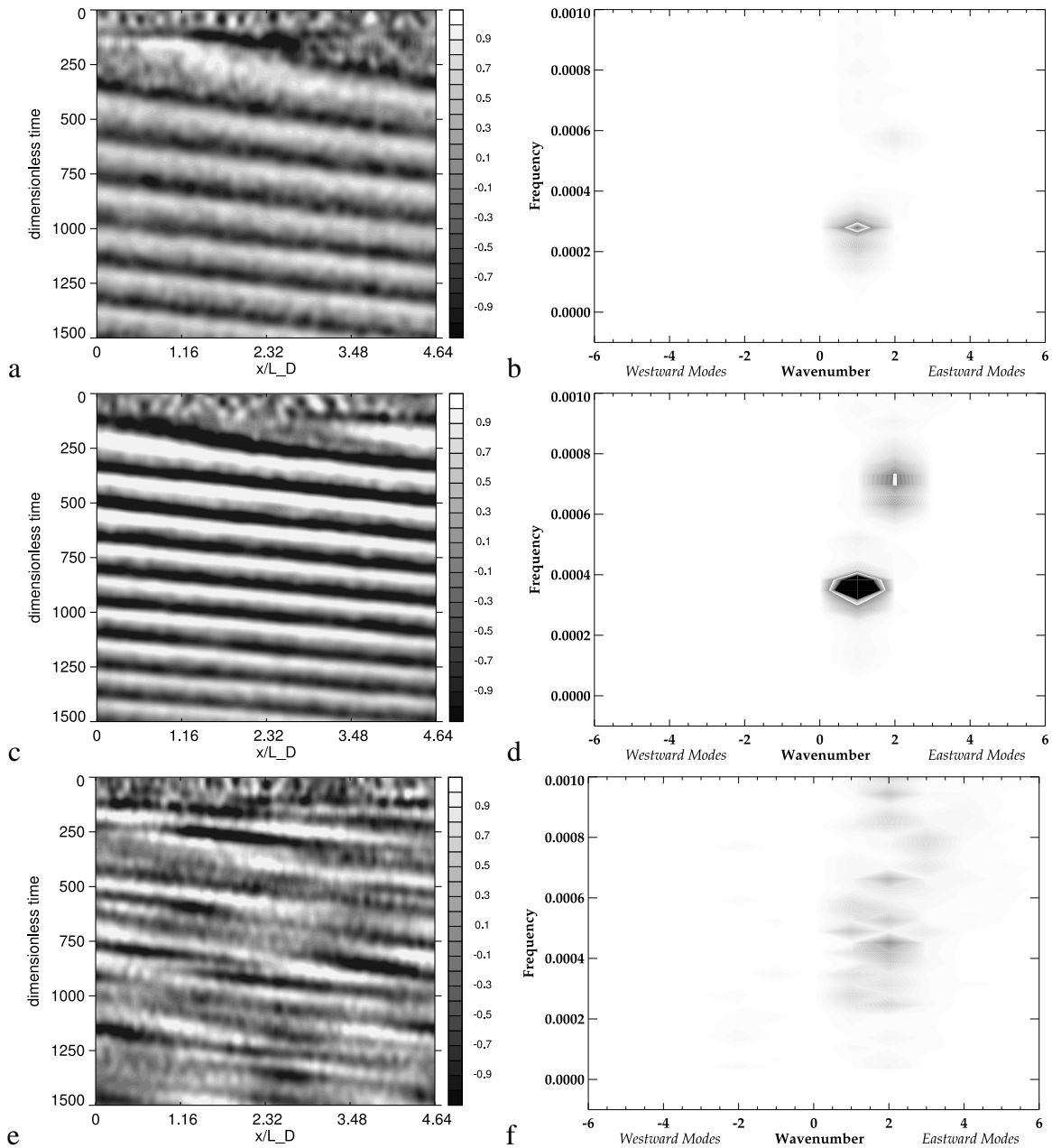


Figure 10: Hovmöller diagram of the temporal anomaly of velocity potential ($\times 10^{-5} \text{ m}^2 \text{ s}^{-1}$) at $0.4H_0$ and the corresponding wavenumber-frequency diagram of velocity potential at the same height as in Fig. 5 but for the simulation of a stably stratified flow with (a-b) no bottom boundary layer heating ($\mathcal{F}_p = 0$), (c-d) moderate ($3\times$) bottom boundary layer heating, and (e-f) strong ($6\times$) bottom boundary layer heating, respectively. The simulation with weak ($1\times$) bottom boundary layer heating is shown in Fig. 5.

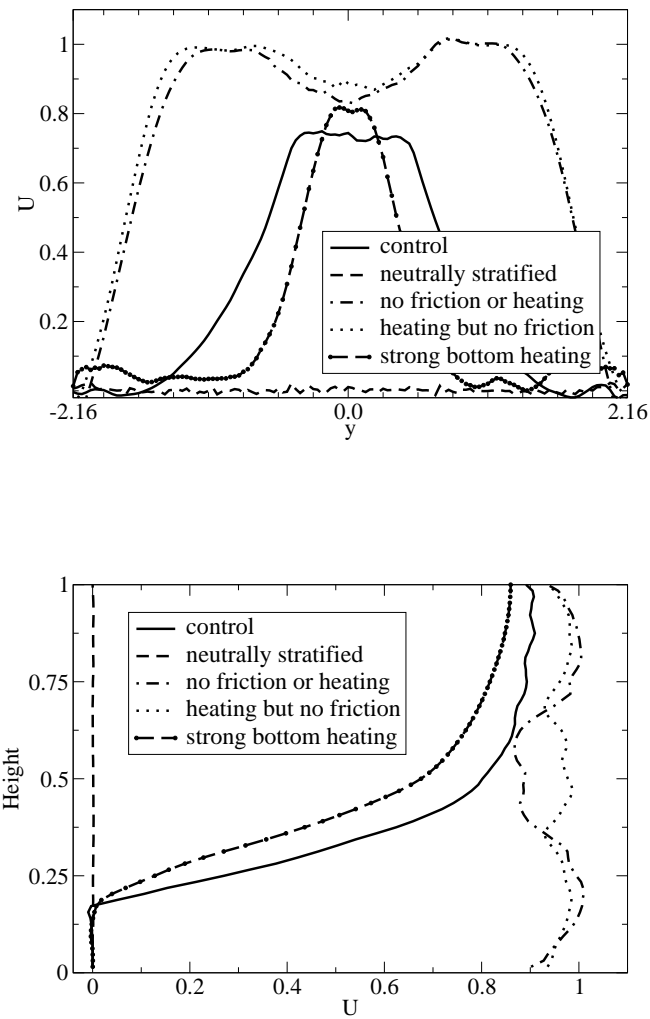


Figure 11: Characteristic zonally averaged zonal flow (upper panel) for selected simulations. The lower panel shows a meridionally averaged vertical profile ($\pm 0.844L_D$ from the mid-channel $y = 0$) of the zonally averaged zonal flow.

Altering the forcing described in (11) by applying a frequency shift in the translation of only one boundary — such that the boundary meander is no longer phase-locked — produces a propagating eastward anomaly that is more episodic, thus indicating the strengthening effect of the signal when a coherent pulsation and translation at both boundaries exists. Increasing the amplitude of the boundary meander ($a/L = 0.2$) leads to a more episodic appearance of solitary structures with a weaker amplitude and a faster propagation speed. Ultimately it leads to the disappearance of the wavenumber one signal with larger forcing amplitude a . Decreasing the amplitude ($a/L = 0.025$) produces a marked solitary structure with a slower propagation speed ($T^* \approx 300$), whereas at smaller amplitude ($a/L = 0.005$) several Rossby waves but no coherent wavenumber one solitary structure is observed. The solution dependence on the forcing amplitude substantiates the nonlinear perspective on the dynamics of the MJO, advocated in this paper. Interestingly, these sensitivities are consistent with eastward propagating convective anomalies found in aquaplanet simulations with the IFS — used in the operational global NWP applications at ECMWF — conducted by the first author using sea surface temperature (SST) gradients further away and closer to the equator (Neale and Hoskins, 2000), respectively. Furthermore, it is found that a boundary forcing wavelength closer to the internal Rossby radius of deformation L_D is the most effective way to obtain long-lived coherent structures. In the above simulations, $x_0/s \approx 0.77L_D$; simulations with $x_0/s = L_D$ similarly produce persistent solitary waves. In contrast, a boundary forcing wavelength $x_0/s = 0.1L_D$ did not lead to solitary structures even after long time. This result suggests a resonance effect of the system with respect to length-scales $\mathcal{O}(L_D)$, which is consistent with weakly nonlinear theory of Rossby solitary waves; cf. Boyd (1980).

4 Discussion

Section 3 presents evidence how episodic solitary structures emerge and propagate in an idealized setting on the equatorial β -plane. The sensitivity experiments indicate the essential role of the propagating meridional boundary meander to precondition the background flow in such a way that it supports the occurrence and persistence of a solitary wave. Given the extraordinary persistence of the solitary wave structure in the laboratory-scale simulations, even when the meander was stopped and despite the presence of the frictional bottom boundary layer, suggests the alternative possibility that in the tropical atmosphere, perhaps only initially extratropical influences play a decisive role in the formation of an MJO event.

The effect of stratification is measured by the ratio $\mathcal{S}^2 = (L_D/L)^2 = SH_0\text{Ro}^2/\text{Fr}^2$ with $S = N^2/g$. For a given Rossby and flow Froude number strong stratification is found to be an essential pre-requisite for the nonlinear evolution of slow moving solitary Rossby waves in three dimensions. However, for either neutral ($S = 0 \text{ m}^{-1}$), weak ($S = 1. \times 10^{-4} \text{ m}^{-1}$) or even moderate ($S = 1. \times 10^{-2} \text{ m}^{-1}$) stratification and $\mathcal{F}^j \equiv \mathcal{F}_\rho \equiv 0$ a fairly fast eastward propagating anomaly is observed, similar (also in horizontal structure) to the 2D case. In contrast, with heating or boundary layer friction included, only the simulations with strong stratification result in a slow moving Rossby solitary wave, whereas all other simulations are dominated by short-scale, convective patterns without any coherent propagation. Interestingly, for strong stratification, which implies $N \gg f$ (Gill, 1982, p.449), the mechanism of vortex stretching is essentially eliminated and the motions are governed by a conservation equation for absolute vorticity $\nabla^2\psi + f$ (Pedlosky, 1987, p.360). The dependence on strong vertical stratification thus provides a reason why Rossby solitary waves have so far not been clearly identified in the well-mixed upper layer of tropical oceans, either observationally or in general circulation models (Boyd, 2002).

In the absence of both heating and boundary layer friction ($\mathcal{F}^j \equiv \mathcal{F}_\rho \equiv 0$), and despite stable stratification $S = 0.25 \text{ m}^{-1}$ (discussed earlier) the solitary wave appears unstable and an initially formed lower frequency signal (just after the boundary meander started) dies out quickly. Despite a strong meridional shear, the simulation shows no vertical zonal mean wind shear, a prerequisite for the energy transfer between barotropic and

baroclinic equatorial wave-packets described in [Majda and Biello \(2003\)](#). The inclusion of bottom friction is found to significantly effect the vertical shear of zonal mean wind potentially aiding the formation of solitary structures. However, the boundary conditions imposed at $z = 0, H_0$ appear to pre-condition the vertical mode selection such that it may also weaken the amplitude or eliminate the occurrence of solitary waves.

The reduced equations of [Majda and Biello \(2003\)](#) and [Biello and Majda \(2004a\)](#) have been extended in [Biello and Majda \(2004b\)](#) to include the effect of boundary layer friction by considering the dynamics of the Ekman layer (cf. [Pedlosky \(1987\)](#) p.185) and thermal dissipation. They conclude that the energy transfer between (extratropical) barotropic and (equatorially trapped) baroclinic wave packets is not significantly altered by dissipation. In particular, “strong coherent structures which form are less effected by dissipation of mean flows since their energy transfer tends to be through direct wave-wave interaction” ([Biello and Majda, 2004b](#)). This finding is broadly in agreement with the laboratory-scale β -plane simulations that exhibit extraordinary persistence and no diminishing of the initial amplitude in the presence of bottom boundary layer friction. Notably, in the simulations the time-scale of the viscous boundary layer friction is shorter than the Ekman time-scale.

The enhanced upward and downward motions within the solitary envelope are particularly strong in the absence of the bottom boundary layer friction, cf. [Fig. 9](#). The idealized numerical experiments in [section 3](#) thus address both the dry and the convectively active phase of an MJO event. The vertical motions are clearly organized within the solitary envelope and also outside of it, cf. [Figs. 4 and 9](#), whereas in the absence of a solitary wave random convective patterns prevail. The 3D equation (1) in [section 2](#) entails a strongly two-dimensional character and thus does not explain this enforcement of the vertical motions in the way seen in the simulations. However, the behavior is consistent with the observations of the structure of individual equatorial MJO events, and it is a robust result of our 3D nonlinear numerical simulations. Theoretical investigations ([Moncrieff, 2004](#); [Majda and Biello, 2004](#); [Biello et al., 2007](#)) suggest the importance of a vertically tilted structure and an associated upscale momentum flux towards larger scales for the MJO maintenance. Observations of the MJO appear to support a westward vertical tilt of zonal wind for the Pacific region but not for the Indian Ocean region ([Kiladis et al., 2005](#)). In the ILES experiments described in this paper we note a distinct westward tilt of the zonal wind anomalies associated with the fully developed solitary structure in the simulations with heating and no bottom boundary layer friction. However, in the simulations with boundary layer friction included, the zonal wind anomalies show no significant vertical tilt.

The laboratory-scale results may be extrapolated to the equatorial atmosphere (cf. [Table 1](#)). The effect of stratification is measured by the ratio $(L_D/L)^2$ which is $\mathcal{O}(1)$ for both the solitary structures in the laboratory-scale simulations and for the typical length-scale L of the equatorial MJO. Both [Charney \(1963\)](#) and [Yano and Bonazzola \(2009\)](#) stress the strongly stratified character of the large-scale tropical environment, which favors the evolution of nonlinear equatorial Rossby waves in the way discussed earlier. Quasi-non-divergent flow, driven primarily by coupling with e.g. extratropical motions ([Charney, 1963](#)), can co-exist with the commonly accepted view of planetary-scale tropical motions, with linear equatorial waves modulated by diabatic heating ([Matsuno, 1966](#); [Wheeler and Kiladis, 1999](#); [Yano and Bonazzola, 2009](#); [Biello and Majda, 2005](#)). In this sense, the MJO may be understood as a quasi-horizontal and quasi-non-divergent, synoptic-scale tropical motion that persists at planetary scale due to nonlinearity, and that is governed by a particular solution of the conservation equation for absolute vorticity $\nabla^2\psi + f$.

The period in our simulations is a function of the domain size as well as the propagation speed and the relative size of the solitary structure and its amplitude. Incidentally, if the nondimensionalized period $T^* = 194$ — as typically obtained from the laboratory-scale simulations — is rescaled for the tropical atmosphere one obtains a propagation speed of the solitary structure of 5.7 ms^{-1} , which agrees well with the observational record of the MJO ([Zhang, 2005](#)). An analysis of the power spectra of re-analysis data from ERA40 ([Uppala et al.,](#)

2005) zonal mean zonal wind⁹ at 200hPa or at 500hPa shows a statistically robust deviation from an artificially created red noise spectrum in the range 20-60 days (Wedi, 2004). Altogether this suggests that the MJO period is variable and not uniquely defined by its propagation speed.

5 Conclusions

The hypothesis has been tested that eastward propagating MJO-like structures originate fundamentally as a result of nonlinear (dry) Rossby wave dynamics. The series of numerical experiments vindicate the nonlinear perspective on the dynamics of the MJO. In particular, the β -plane model in section 3.1 reproduces eastward propagating solitary structures in 2D and 3D simulations, given propagating meanders are applied at the meridional boundaries. The reductionistic β -plane model stresses the importance of the β -effect for the eastward propagation and the importance of strong stratification in the presence of boundary layer heating or friction for the occurrences of solitary structures that subsequently determine the organization of convection. Neutral stratification is found to be a sufficient condition for the extinction of a solitary structure. Vertical and meridional shear of the zonal mean zonal wind are not sufficient conditions for the occurrence of a low frequency signal. However, a meridional shear of the zonal mean zonal wind appears to be a necessary condition for a solitary structure to occur. The boundary conditions imposed at $z = 0, H_0$ are found to substantially influence the vertical mode selection and can contribute to the suppression of the solitary wave itself. Furthermore, excessive heating or boundary layer friction may eliminate a coherent low-frequency signal. Interestingly, the permanence of solitary structures has been shown to persist beyond the validity of the quasi-geostrophic theory based on an expansion for small Rossby number, upto $Ro \rightarrow 1$, which thus includes the synoptic-scale regime developed in the scale analysis of Charney (1963).

The main goal of this paper was to demonstrate the fundamental role of resonant nonlinear wave dynamics for the origin and evolution of periodically reoccurring anomalous flow patterns in the equatorial troposphere. As a result, the MJO may be understood as a quasi-horizontal and quasi-non-divergent synoptic-scale motion that is driven, or rather preconditioned, by coupling with extratropical weather, and that persists at planetary scale due to nonlinearity. This motion is governed by a particular solution of the conservation law for absolute vorticity $\nabla^2\psi + f$ (Charney, 1963). Consequently, the process of convection is found to be important but chronologically secondary to the MJO evolution. A case study of an individual MJO event (Hsu et al., 1990) supports this view. However, given the study in Matthews (2008) there may exist more than one MJO mechanism in the tropical atmosphere.

The authors found further numerical evidence for a robust low-wavenumber and low-frequency signature in the equatorial wave spectra at 600 hPa and 200 hPa of idealized Held-Suarez global climate (Held and Suarez, 1994) experiments on the sphere. Notably, these results were obtained from the dynamical core simulations of two entirely different GCMs, IFS and EULAG. The results compare also well with analyzed ERA40 data of individual MJO events, where velocity potential anomalies are found to exist long before substantial convection develops. Case studies of individual MJO events reported in Hsu et al. (1990) and more recently in Ray et al. (2009) support the view that the MJO initiation and maintenance — at least for some MJO events — is a global problem. These findings corroborate the results of this paper.

Acknowledgements: We would like to thank Thomas Jung for his help with analyzing the data. Peter Bechtold and Jun-Ichi Yano are gratefully acknowledged for stimulating discussions and reviewing the manuscript. We thank Mitch Moncrieff, a further anonymous referee and the editor Shigeo Yoden for their valuable comments that helped to improve the manuscript.

⁹averaged between ± 10 degrees latitude over 35 years

References

- Biello, J., and A. Majda, 2004a: The effect of meridional and vertical shear on the interaction of equatorial baroclinic and barotropic waves. *Studies in Applied Mathematics*, **112**, 341–390.
- , and —, 2004b: Boundary layer dissipation and the nonlinear interaction of equatorial baroclinic and barotropic Rossby waves. *Geophys. Astrophys. Fluid Dynamics*, **98**, 85–127.
- , and —, 2005: A new multiscale model for the Madden-Julian oscillation. *J. Atmos. Sci.*, **62**, 1694–1721.
- Biello, J., A. J. Majda, and M. Moncrieff, 2007: Meridional momentum flux and superrotation in the multiscale IPESD MJO model. *J. Atmos. Sci.*, **64**, 1636–1651.
- Boyd, J., 1980: Equatorial solitary waves. part I: Rossby solitons. *J. Phys. Oceanogr.*, **10**, 1699–1717.
- 2002: Equatorial solitary waves. part V: Initial value experiments, coexisting branches, and tilted-pair instability. *J. Phys. Oceanogr.*, **32**, 2589–2602.
- Boyd, J. P., and G.-Y. Chen, 2001: Weakly nonlinear wavepackets in the Korteweg-deVries equation: The KDV/NLS connection. *Mathematics and Computers in Simulation*, **55**, 317–328.
- Charney, J., 1963: A note on large-scale motions in the tropics. *J. Atmos. Sci.*, **20**, 607–609.
- Chen, T.-C., and J.-M. Chen, 1997: On the relationship between the streamfunction and velocity potential of the Madden-Julian oscillation. *J. Atmos. Sci.*, **54**, 679685.
- Delayen, K., and J.-I. Yano, 2009: Is asymptotic non-divergence of the large-scale tropical atmosphere consistent with equatorial wave theories ? *Tellus*, doi:10.1111/j.1600-0870.2009.00404.x.
- Dodd, R., J. Eilbeck, J. Gibbon, and H. Morris, 1982: *Solitons and Nonlinear Wave equations*. Academic Press, London.
- Domaradzki, J., Z. Xiao, and P. Smolarkiewicz, 2003: Effective eddy viscosities in implicit large eddy simulations of turbulent flows. *Phys. Fluids*, **15**, 3890–3893.
- ECMWF: 2003. *ECMWF/CLIVAR Workshop*, Eur. Cent. For Medium-Range Weather Forecasts, Reading, UK, Proc. 2003 ECMWF/CLIVAR Workshop on Simulation and Prediction of Intra-Seasonal Variability with emphasis on the MJO.
- Flierl, G., 1987: Isolated eddy models in geophysics. *Ann. Rev. Fluid Mech.*, **19**, 493–530.
- Fu, Z.-T., S.-K. Liu, and S.-D. Liu, 2005: Equatorial Rossby solitary wave under the external forcing. *Commun. Theor. Phys.*, **43**, 45–48.
- Gill, A., 1980: Some simple solutions for heat-induced tropical circulation. *Q.J.R. Meteorol. Soc.*, **106**, 447–462.
- Gill, A., 1982: *Atmosphere-Ocean Dynamics*, volume 30 of *International Geophysics series*. Academic Press, London.
- Hartmann, D. L., and H. H. Hendon, 2007: Resolving an atmospheric enigma. *Science*, **318**, 1731–1732.
- Held, I., and M. Suarez, 1994: A proposal for the intercomparison of the dynamical cores of atmospheric general circulation models. *Bull. Am. Meteorol. Soc.*, **73**, 1825–1830.

- Hodyss, D., and T. Nathan, 2002: Solitary Rossby waves in zonally varying jet flows. *Geophys. Astrophys. Fluid Dynamics*, **96**, 239–262.
- Holton, J. R., 1992: *An introduction to dynamic meteorology*, volume 23 of *International Geophysics series*. Academic Press, New York, 3rd edition.
- Hoskins, B. J., and G.-Y. Yang, 2000: The equatorial response to higher latitude forcing. *J. Atmos. Sci.*, **57**, 1197–1213.
- Hsu, H.-H., B. J. Hoskins, and F.-F. Jin, 1990: The 1985/86 intraseasonal oscillation and the role of the extratropics. *J. Atmos. Sci.*, **47**, 823–839.
- Kartashova, E., and V. S. L’vov, 2007: Model of intraseasonal oscillations in the Earth’s atmosphere. *Phys. Rev. Letters*, **98**, 1–4.
- Kiladis, G., K. Straub, and P. Haertel, 2005: Zonal and vertical structure of the Madden-Julian oscillation. *J. Atmos. Sci.*, **62**, 2790–2809.
- Kiladis, G. N., and M. Wheeler, 1995: Horizontal and vertical structure of observed tropospheric equatorial Rossby waves. *J. Geophys. Res.*, **100**, 22981–22997.
- Kuo, H. L., 1972: On a generalized potential vorticity equation for quasi-geostrophic flow. *Pure and Applied Geophysics*, **96**, 171–175.
- Lin, J.-L., M.-I. Lee, D. Kim, I.-S. Kang, and D. M. Frierson, 2008: The impacts of convective parametrization and moisture triggering on AGCM-simulated convectively coupled equatorial waves. *J. Climate*, **21**, 883–909.
- Madden, R. A., and P. R. Julian, 1971: Detection of a 40-50 day oscillation in the zonal wind in the tropical Pacific. *J. Atmos. Sci.*, **28**, 702–708.
- , and —, 1972: Description of global scale circulation cells in the Tropics with 40-50 day period. *J. Atmos. Sci.*, **29**, 1109–1123.
- Maicun, L., 1987a: Equatorial solitary waves of tropical atmospheric motion in shear flow. *Adv. Atmos. Sci.*, **4**, 125–136.
- 1987b: On the low-frequency, planetary-scale motion in the tropical atmosphere and oceans. *Adv. Atmos. Sci.*, **4**, 249–263.
- Majda, A. J., and J. Biello, 2003: The nonlinear interaction of barotropic and equatorial baroclinic Rossby waves. *J. Atmos. Sci.*, **60**, 1809–1821.
- , and —, 2004: A multiscale model for tropical intraseasonal oscillations. *Proc. Natl. Acad. Sci.*, **101**, 4736–4741.
- Mak, M.-K., 1969: Laterally driven stochastic motions in the tropics. *J. Atmos. Sci.*, **26**, 41–64.
- Malanotte-Rizzoli, P., 1980: Solitary Rossby waves over variable relief and their stability. part II: numerical experiments. *Dyn. Atm. Ocean*, **4**, 261–294.
- Malanotte-Rizzoli, P., D. B. Haidvogel, and R. E. Young, 1987: Numerical simulation of transient boundary-forced radiation. part I: The linear regime. *J. Phys. Oceanogr.*, **17**, 1439–1457.

- Malanotte-Rizzoli, P., R. E. Young, and D. B. Haidvogel, 1988: Numerical simulation of transient boundary-forced radiation. part II: The Modon regime. *J. Phys. Oceanogr.*, **18**, 1546–1569.
- Margolin, L. G., W. J. Rider, and F. F. Grinstein, 2006: Modeling turbulent flow with implicit les. *J. Turbul.*, **7**, 1–27.
- Matsuno, T., 1966: Quasi-geostrophic motions in the equatorial area. *J. Meteor. Soc. Japan*, **44**, 25–43.
- Matthews, A. J., 2008: Primary and successive events in the Madden-Julian oscillation. *Q.J.R. Meteorol. Soc.*, **134**, 439–453.
- Miura, H., M. Satoh, T. Nasuno, A. T. Noda, and K. Oouchi, 2007: A Madden-Julian oscillation event realistically simulated by a global cloud-resolving model. *Science*, **318**, 1763–1765.
- Moncrieff, M. W., 2004: Analytic representation of the large scale organization of tropical convection. *J. Atmos. Sci.*, **61**, 1521–1538.
- Neale, R. B., and B. J. Hoskins, 2000: A standard test for AGCMs and their physical parameterizations. I: The proposal. *Atmos. Sci. Letters*, **1**, 101–107.
- Pedlosky, J., 1987: *Geophys. Fluid Dynamics*, Springer Verlag, New York. second ed. edition.
- Phillips, O. M., 1981: Wave interactions - the evolution of an idea. *J. Fluid Mech.*, **106**, 215–227.
- Piotrowski, Z. P., P. K. Smolarkiewicz, S. P. Malinowski, and A. Wyszogrodzki, 2009: On numerical realizability of thermal convection. *J. Comput. Phys.*, **228**, 6268–6290.
- Plumb, R. A., and R. C. Bell, 1982: A model of the quasi-biennial oscillation on an equatorial beta plane. *Q.J.R. Meteorol. Soc.*, **108**, 335–352.
- Plumb, R. A., and D. McEwan, 1978: The instability of a forced standing wave in a viscous stratified fluid: A laboratory analogue of the quasi-biennial oscillation. *J. Atmos. Sci.*, **35**, 1827–1839.
- Prusa, J. M., and P. K. Smolarkiewicz, 2003: An all-scale anelastic model for geophysical flows: Dynamic grid deformation. *J. Comput. Phys.*, **190**, 601–622.
- Prusa, J. M., P. K. Smolarkiewicz, and A. A. Wyszogrodzki, 2008: EULAG, a computational model for multi-scale flows. *Comput. Fluids*, **37**, 1193–1207.
- Ray, P., C. Zhang, J. Dudhia, and S. S. Chen, 2009: A numerical case study on the initiation of the Madden-Julian oscillation. *J. Atmos. Sci.*, **66**, 310–331.
- Redekopp, L., 1977: On the theory of solitary Rossby waves. *J. Fluid Mech.*, **82**, 725–745.
- Rossby, C.-G., 1940: Planetary flow patterns in the atmosphere. *Q.J.R. Meteorol. Soc.*, **66**, 68–87.
- Saujani, S., and T. G. Shepherd, 2006: A unified theory of balance in the extratropics. *J. Fluid Mech.*, **569**, 447–464.
- Smolarkiewicz, P. K., and J. M. Prusa, 2005: Towards mesh adaptivity for geophysical turbulence: Continuous mapping approach. *Int. J. Numer. Methods Fluids*, **47**, 789–801.
- Smolarkiewicz, P. K., and J. Szmelter, 2009: Iterated upwind schemes for gas dynamics. *J. Comput. Phys.*, **228**, 33–54.

- Smolarkiewicz, P. K., C. Temperton, S. J. Thomas, and A. A. Wyszogrodzki: 2004, Spectral preconditioners for nonhydrostatic atmospheric models: extreme applications. Eur. Cent. For Medium-Range Weather Forecasts, Reading, UK, Proc. 2004 Seminar on Recent Developments in Numerical Methods for Atmosphere and Ocean Modelling, 203–220.
- Straub, K., 2003: Extratropical forcing of convectively coupled Kelvin waves during austral winter. *J. Atmos. Sci.*, **60**, 526–543.
- Strauss, D. M., and R. Lindzen, 2000: Planetary-scale baroclinic instability and the MJO. *J. Atmos. Sci.*, **57**, 3609–3626.
- Tuyl, A. V., 1987: Nonlinearities in low-frequency equatorial waves. *J. Atmos. Sci.*, **44**, 2478–2492.
- Uppala, S. M., P. W. Kallberg, A. J. Simmons, U. Andrae, V. da Costa Bechtold, M. Fiorino, J. K. Gibson, J. Haseler, A. Hernandez, G. A. Kelly, X. Li, K. Onogi, S. Saarinen, N. Sokka, R. P. Allan, E. Andersson, K. Arpe, M. A. Balmaseda, A. C. M. Beljaars, L. van de Berg, J. Bidlot, N. Bormann, S. Caires, F. Chevallier, A. Dethof, M. Dragosavac, M. Fisher, M. Fuentes, S. Hagemann, E. Holm, B. J. Hoskins, L. Isaksen, P. A. E. M. Janssen, R. Jenne, A. P. McNally, J.-F. Mahfouf, J.-J. Morcrette, N. A. Rayner, R. W. Saunders, P. Simon, A. Sterl, K. E. Trenberth, A. Untch, D. Vasiljevic, P. Viterbo, and J. Woollen, 2005: The ERA-40 re-analysis. *Quart. J. Roy. Meteor. Soc.*, **131**, 2961–3012.
- Verkley, W., 2009: A balanced approximation of the one-layer shallow water equations on a sphere. *J. Atmos. Sci.*, **66**, 1735–1748.
- Wedi, N. P.: 2004, Numerical simulation of internal gravity wave dynamics. Eur. Cent. For Medium-Range Weather Forecasts, Reading, UK, Proc. ECMWF Workshop on Recent Developments in numerical methods for atmosphere and ocean modelling, 221–232.
- Wedi, N. P., and P. K. Smolarkiewicz, 2004: Extending Gal-Chen & Somerville terrain-following coordinate transformation on time-dependent curvilinear boundaries. *J. Comput. Phys.*, **193**, 1–20.
- , and —, 2005: Laboratory for internal gravity-wave dynamics: The numerical equivalent to the quasi-biennial oscillation (QBO) analogue. *Int. J. Numer. Methods Fluids*, **47**, 1369–1374.
- , and —, 2006: Direct numerical simulation of the Plumb-McEwan laboratory analog of the QBO. *J. Atmos. Sci.*, **63**, 3226–3252.
- , and —, 2008: A reduced model of the Madden-Julian oscillation. *Int. J. Numer. Methods Fluids*, **56**, 1583–1588.
- , and —, 2009: A framework for testing global nonhydrostatic models. *Q.J.R. Meteorol. Soc.*, **135**, 469–484.
- Wheeler, M., and G. N. Kiladis, 1999: Convectively coupled equatorial waves: Analysis of clouds and temperature in the wave number-frequency domain. *J. Atmos. Sci.*, **56**, 374–399.
- Yano, J.-I., and M. Bonazzola, 2009: Scale analysis for the large-scale tropical atmospheric dynamics. *J. Atmos. Sci.*, **66**, 159–172.
- Yano, J.-I., S. Mulet, and M. Bonazzola, 2009: Tropical large-scale circulations: asymptotically nondivergent? *Tellus*, **66**, 417–427.
- Yano, J.-I., J. J. Tribbia, and F. Reichmann, 1997: Jovian vortex dynamics from a historical perspective. CP414 Research Workshop: Two-dimensional turbulence in Plasmas and Fluids, 155–172.



- Zagar, N., E. Andersson, and M. Fisher, 2005: Balanced tropical data assimilation based on a study of equatorial waves in ECMWF short-range forecast errors. *Q.J.R. Meteorol. Soc.*, **131**, 987–1011.
- Zhang, C., 2005: Madden-Julian Oscillation. *Rev. Geophys.*, **43**, RG2003, doi:10.1029/2004RG000158.
- Zou, J., and H.-R. Cho, 2000: A nonlinear Schroedinger equation model of the intraseasonal oscillation. *J. Atmos. Sci.*, **57**, 2435–2444.